Some Aspects of Circulation and Climate over the Eastern Equatorial Atlantic

STEFAN HASTENRATH AND PETER LAMB[1]

Department of Meteorology, University of Wisconsin, Madison 53706

(Manuscript received 14 March 1977, in revised form 2 May 1977)

ABSTRACT

The South Atlantic trades cross the equator at the height of northern summer, recurving from southeasterly to southwesterly near 5°N, and undercut the northeast trades along an extended discontinuity. The negative surface stress curl of this atmospheric current leads to upwelling and a cold ocean surface immediately south of the equator, with downwelling and higher sea temperatures to the north. This clockwise turning, cross-equatorial flow is markedly divergent between the equator and about 5°N. A band of convergence extends poleward from 5°N into the southern fringe of the northeast trades. Maximum convergence, cloudiness and precipitation frequency all occur ~350 km south of the surface wind discontinuity and pressure minimum, in a region of high directional steadiness of wind.

1. Introduction

The atmosphere over West Africa and the adjacent Atlantic has received increased attention in recent years in connection with the GATE field program. However, some disagreement has developed concerning the structure of the complex of semi-permanent atmospheric and oceanic features in this area. A widely held view is that the surface pressure trough, the surface wind discontinuity and the belts of maximum sea surface temperature (SST), convergence, cloudiness and precipitation all coincide in what is commonly referred to as the Intertropical Convergence Zone (ITCZ) [see review in Ramage (1974)]. To some, the ITCZ is the locus of most frequent traveling disturbances [review in Lockwood (1974, pp. 89–93)]. These interpretations are not universally accepted. For instance, Ramage (1974) and Sadler (1975) suggest that the convergence-cloudiness-rainfall maximum is separate from the zone of minimum surface pressure and maximum SST. The present paper analyzes recently available long-term surface data and limited upper air data for July and August, with a view to obtaining a better understanding of the circulation and climate in the equatorial Atlantic-West African domain. Surface charts for all calendar months (Hastenrath and Lamb, 1977) show July–August to possess a number of unique characteristics.

2. Data

Ship observations made in the tropical Atlantic during 1911–70 were obtained from the National Climatic Center, Asheville, N. C., in a 1° latitude-longitude square spatial resolution. About 1.5 million individual observations were available for the ocean area mapped in Fig. 1, with an approximately even distribution over the calendar months. Elements of interest here include sea level pressure, surface wind, SST, cloudiness and precipitation frequency. Fields derived from the wind data include divergence, relative vorticity, curl of the wind stress and oceanic mixed-layer vertical motion. Details of data processing have been given elsewhere (Hastenrath, 1976; Hastenrath and Lamb, 1977). Several years of radiosonde observations for the West African coast were obtained from ASECNA (1969–73). For reasons of data stability, the months of July and August are analyzed together, although a slight northward shift of circulation features takes place during this time.

3. Surface circulation

Salient features of the July–August surface flow over the eastern equatorial Atlantic are mapped in Fig. 1. The dynamics of this surface circulation will be discussed elsewhere, with a descriptive account sufficing here. The southeast trades from the South Atlantic cross the equator and reach a speed maximum near 5°N, where they recurve to southwesterly; further poleward, this clockwise turning, cross-equatorial current meets the northeast trades along an extended zonally oriented discontinuity. There is marked divergence between the equator and about 5°N. A band of convergence extends from here into the southern fringe of the northeast trades, with the strongest convergence

[1] Present affiliation: Department of Geography, University of Adelaide, Adelaide, South Australia 5001, Australia.

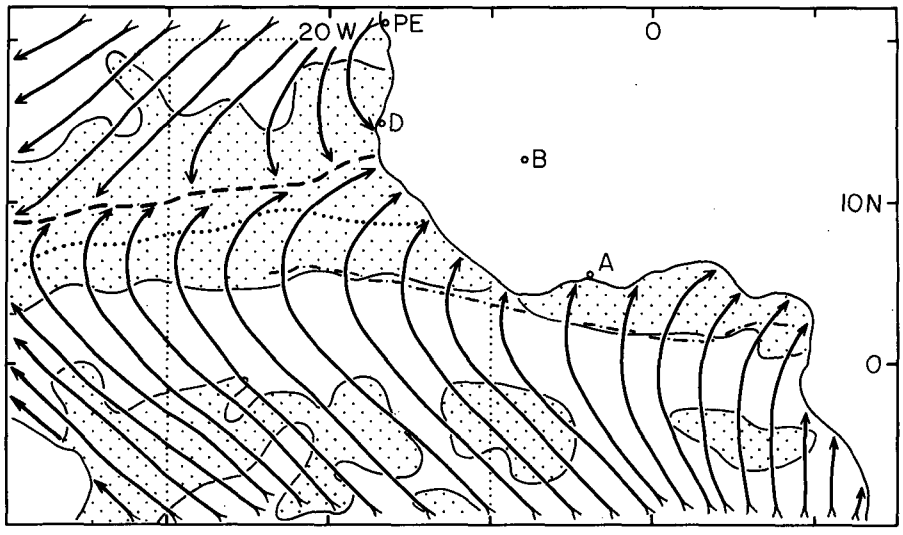

FIG. 1. Surface circulation over the eastern equatorial Atlantic, July/August 1911–70: streamlines, solid lines, surface wind discontinuity, heavy broken line; speed maximum, thin dash-dotted line; convergent areas, stippled; convergence maximum, dotted line. Dotted rectangle is area for which meridional profiles in Figs. 2–4 were computed. PE, D, B and A indicate radiosonde stations Port Etienne, Dakar, Bamako and Abidjan, respectively.

occurring about 350 km south of the surface flow discontinuity.

Figs. 2 and 3 present July–August meridional profiles of indicative atmospheric-oceanic parameters for the rectangle entered into Fig. 1. Both the pressure trough (Fig. 2) and SST maximum (Fig. 3) are broad and contain weak gradients; except near the northern edge of the trough, these features approximately coincide. The maxima of cloudiness, precipitation frequency and convergence are very closely coincident, and lie ~350 km south of the surface flow discontinuity (Fig. 2). This differs from the widely held interpretation of the ITCZ cited in the Introduction, and instead offers support for the alternative structure suggested by Ramage (1974) and Sadler (1975). Comparison of the meridional profiles of resultant and scalar wind speed and divergence shows that the convergence maximum is located within a region of high directional steadiness of wind. In contrast, the low steadiness values near the confluence axis occur beneath less cloud cover. This may support Sadler's (1975) contention that "the mean monthly maximum cloud zone does not coincide with the tracks of migratory vortices," and that "synoptic-scale circulations are not important in producing the maximum cloud zones." It is remembered, however, that surface observations are analyzed here, and that the displacement of cloud clusters may be related to conditions in higher layers.

4. The ocean

The meridional profile of SST in Fig. 3 reveals very cold surface waters immediately south of the equator. A pronounced increase in SST occurs from 0–5°N, with a flat SST maximum extending between 5 and 14°N; the warmest surface water is found near 12°N. SST decreases poleward toward the realm of the cold Canary Current.

Various mechanisms may cooperate in maintaining the above SST pattern. First, lateral advection may be a factor both in the downstream portion of the Canary Current and in the cold water region of the southeastern equatorial Atlantic. Further, wind-induced large-scale upwelling may play a role in the cold tongue immediately to the south of the equator. Two separate mechanisms are considered in the following.

For steady-state ocean conditions away from the immediate vicinity of coasts and the equator, vertical motion near the bottom of the mixed layer can be estimated from (Yoshida and Mao, 1957)

$$w=\frac{1}{\rho f}\left(\frac{\partial \tau_y}{\partial x}-\frac{\partial \tau_x}{\partial y}\right). \tag{1}$$

Here ρ is the density of sea water, f the Coriolis parameter, and τ_x and τ_y are the zonal and meridional components of the surface stress τ with positive vertical velocities for upwelling. It is noted that a negative wind stress curl calls for upwelling in the Southern Hemisphere and downwelling in the Northern Hemisphere, with largest values near the equator; shear terms neglected in the derivation of Eq. (1) conceivably account for continuity.

The field of surface stress was calculated from the wind field using the relation

$$|\tau|=\rho C_D|\mathbf{V}|^2. \tag{2}$$

Values of $\rho = 1.175$ kg m^{-3} and $C_D = 2.8 \times 10^{-3}$ were chosen for air density and drag coefficient, respectively. The average of $|\mathbf{V}|^2$ was approximated by the square of the resultant wind speed, and τ was assumed to have the direction of the resultant wind. As suggested by Roden (1974), a relatively large value of C_D was used to compensate for underestimation of $|\mathbf{V}|^2$ by the above method. In any case, the focus here is on prominent relative patterns rather than absolute magnitudes. The wind stress curl was computed using methods described elsewhere (Hastenrath and Lamb, 1977); the relative vorticity of the surface wind field has a similar pattern.

Fig. 3 presents meridional profiles of the wind stress curl, Coriolis parameter and concomitant ω values yielded by Eq. (1). As can be expected from the flow pattern in Fig. 1, the wind stress curl is negative in a broad region extending from the Southern Hemisphere to about 8°N; positive values occur in the vicinity of the confluence axis. Eq. (1) therefore gives positive values of w (i.e., upward directed) for the Southern Hemisphere, which are particularly large near the equator. In the realm of the clockwise turning, cross-equatorial flow of the Northern Hemisphere, the largest downward motion likewise occurs near the equator. This downwelling decreases northward to near the confluence axis, where the vertical motion changes to weak upwelling. Since strong negative wind stress curl extends from 10°S to 8°N, the mechanism represented by Eq. (1) may contribute to the equatorial SST asymmetry evident in Fig. 3. The possible importance of this mechanism is further underlined by the fact that both the cold tongue immediately south of the equator, and the strong negative wind stress curl of the well-developed, clockwise turning, cross-equatorial surface flow, are confined to the northern summer months (Hastenrath and Lamb, 1977). This is also characteristic of the eastern equatorial Pacific (Hastenrath, 1977; Hastenrath and Lamb, 1977). Thermocline depth in the eastern equatorial Atlantic is about 50 m (Fuglister, 1960, pp. 11–13, 184–185, 204–207). Fig. 3 indicates that the time to cover this vertical distance is of the order of weeks.

A third mechanism, also involving wind-induced vertical motion in the ocean, has been discussed in qualitative terms by Cromwell (1953). He showed that oceanic Ekman transport associated with southeasterly winds could result in divergence and upwelling in a band extending from the Southern Hemisphere to north of the equator, and in an oceanic convergence band at some low latitude in the Northern Hemisphere. This mechanism is interesting in relation to the SST pattern in Fig. 3, which shows the strongest meridional variation north of rather than across the equator.

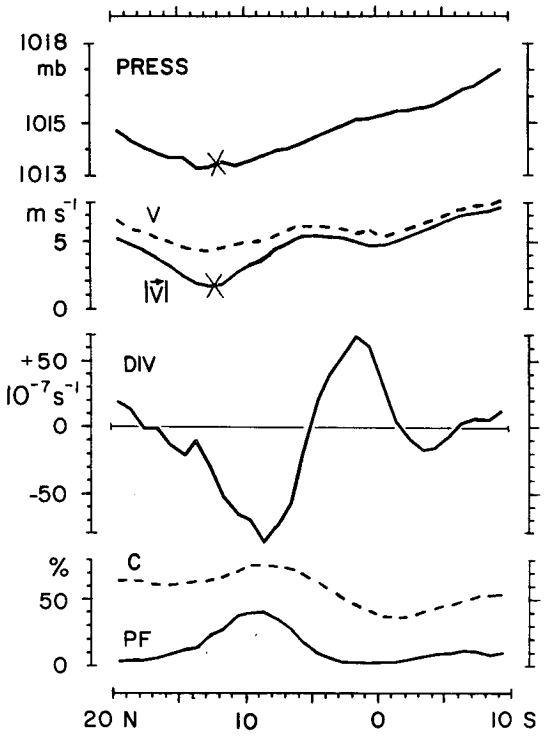

FIG. 2. July/August 1911–70 meridional profiles of sea level pressure, resultant $|\mathbf{V}|$ and scalar wind speed V, divergence, precipitation frequency (PF), and cloudiness (C). Position of surface wind discontinuity is indicated by cross.

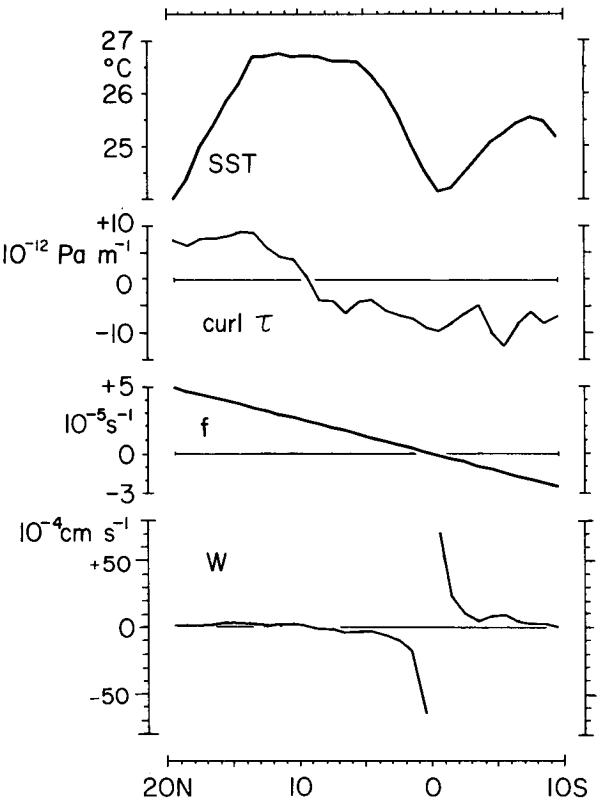

FIG. 3. July/August 1911–70 meridional profiles of sea surface temperature, curl of wind stress, Coriolis parameter f, and vertical motion at bottom of oceanic mixed layer.

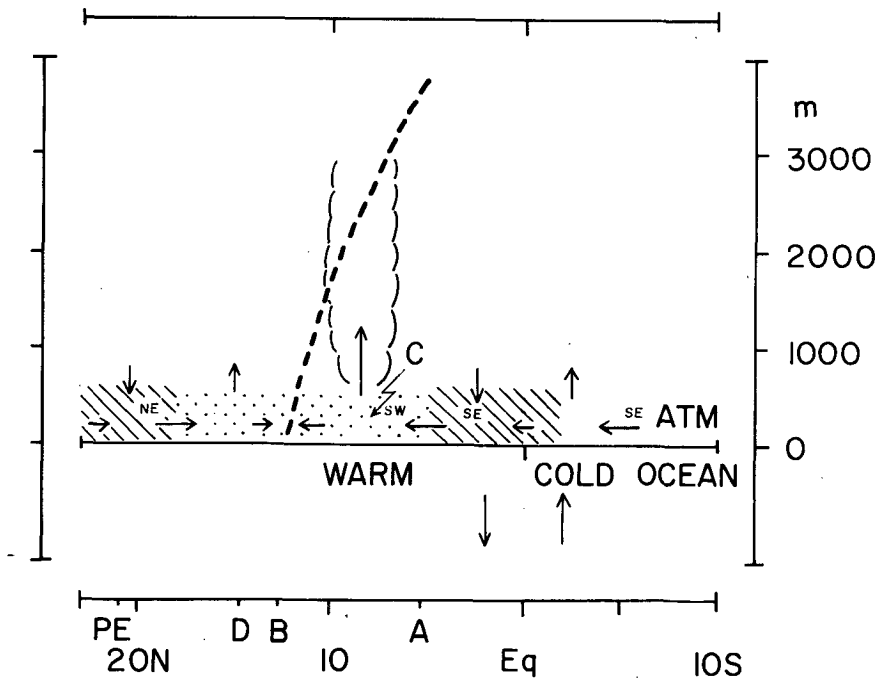

FIG. 4. Meridional-vertical transect for July/August. NE, SE, SW denote wind directions; heavy broken line is discontinuity; hatched areas indicate divergence, stippled areas convergence; C convergence maximum; arrows indicate motion in meridional-vertical plane. PE, D, B and A refer to radiosonde stations indicated in Fig. 1. Vertical exaggeration ~1:550.

The observed SST pattern (Fig. 3) may result from some combination of the mechanisms reviewed above. The SST pattern in turn is expected to be relevant for processes in the lower atmosphere.

5. Vertical structure

A schematic meridional-vertical transect for the equatorial eastern Atlantic–West African sector appears in Fig. 4. This is patterned on earlier transects for the equatorial western Atlantic and eastern Pacific (Hastenrath, 1977). Information on the atmospheric surface layer and the ocean was derived from the aforementioned long-term ship observations. No upper air stations are located within the rectangular ocean area entered into Fig. 1. The slope of the large-scale interface between the lower tropospheric southwesterly current and the northeasterlies aloft was drawn from radiosonde data for stations along the coast of West Africa (ASECNA, 1969–73), and is broadly consistent with values known for the African continent (Leroux, 1970). The interface slope in Fig. 4 is intended only as a general orientation. Atmospheric vertical motion was inferred from the lower tropospheric vergence pattern.

6. Conclusions

The July–August cross-equatorial flow is markedly divergent from the equator to near 5°N, in which vicinity it recurves from southeasterly to southwesterly. A band of convergence extends further poleward into the southern fringe of the northeast trades. However, the maximum convergence occurs about 350 km south of the surface wind discontinuity in a region of high directional steadiness of wind. This suggests that the convergence is primarily associated with the basic flow, rather than migratory disturbances. The cross-equatorial flow undercuts the northeast trades, with the latitude of the surface discontinuity and the inclination of the interface increasing toward northern summer (Leroux, 1970).

The cold ocean surface to the south of the equator (Fig. 3) is unfavorable for convection. A warmer underlying ocean exists between 0–5°N, but here the marked divergence of the lower tropospheric flow would mitigate against convection and cloud development. A region of scarce cloudiness near or somewhat to the south of the equator is commonly apparent in satellite imagery.

This arrangement of semi-permanent near-equatorial atmospheric and oceanic features differs from the conventional interpretation of the Intertropical Convergence Zone in that the maximum convergence-cloudiness-rainfall stays ~350 km south of the surface confluence axis and pressure minimum, and appears essentially associated with the basic flow. The existence of a divergence band to the north of the equator and a speed maximum at the recurvature latitude near 5°N do not seem to have received attention in earlier work.

On the synoptic time scale, the nature of migratory vortices, their preferred tracks, and the arrangement of strongest convergence and weather relative to the vortex center are of particular interest in terms of their contribution to the average pattern. Case studies from the GATE field program may furnish an improved observational basis, although satellite-derived cloud drift for the lower and mid-troposphere is intrinsically unavailable in the zone of most intense convergence and cloudiness. It is hoped that the present paper may provide a useful frame of reference on the climatic time scale.

Acknowledgments. This study was supported by the Climate Dynamics Program of the National Science Foundation.

REFERENCES

ASECNA, 1969–73: Radiosondages 1968–72. Agence pour la Sécurité de la Navigation Aérienne en Afrique et à Madagascar (ASECNA), Direction de l'exploitation Meteorologique, Dakar.

Cromwell, T., 1953: Circulation in a meridional plane in the central equatorial Pacific. *J. Mar. Res.*, **12**, 196–213.

Fuglister, F. C., 1960: *Atlantic Ocean Atlas of Temperature and Salinity Profiles and Data from IGY 1957–58*, Vol. 1. Woods Hole Oceanographic Institution Atlas Series, Woods Hole, Mass., 209 pp.

Hastenrath, S., 1976: Variations in low-latitude circulation and extreme climatic events in the tropical Americas. *J. Atmos. Sci.*, **33**, 202–215.

——, 1977: On the upper-air circulation over the equatorial Americas. *Arch. Meteor. Geophys. Bioklim.*, **A25**, 309–321.

——, and P. Lamb, 1977: *Climatic Atlas of the Tropical Atlantic and Eastern Pacific Ocean*. University of Wisconsin Press, 112 pp.

Leroux, M., 1970: La dynamique des précipitations en Afrique Occidentale. Notes de la Direction de l'Exploitation Météorologique, No. 39, ASECNA, Dakar.

Lockwood, J. G., 1974: *World Climatology, an Environmental Approach*. Arnold, 330 pp.

Ramage, C. S., 1974: Structure of an oceanic near-equatorial trough deduced from research aircraft traverses. *Mon. Wea. Rev.*, **102**, 754–759.

Roden, G. I., 1974: Thermohaline structure, fronts, and sea-air energy exchange of the trade wind region east of Hawaii. *J. Phys. Oceanogr.*, **4**, 168–182.

Sadler, J. C., 1975: The monsoon circulation and cloudiness over the GATE area. *Mon. Wea. Rev.*, **103**, 369–387.

Yoshida, K., and H.-L. Mao, 1957: A theory of upwelling of large horizontal extent. *J. Mar. Res.*, **16**, 40–54.